# Green light emission in silicon through slow-light enhanced third-harmonic generation in photonic-crystal waveguides

B. Corcoran, Christelle Monat, C. Grillet, D. Moss, B. Eggleton, T. White, L. O'Faolain, T. Krauss

# Green light emission in silicon via slow light enhanced third-harmonic generation in photonic crystal waveguides

**B. Corcoran, C. Monat*, C. Grillet, D. J. Moss, B. J. Eggleton**
*CUDOS, Institute for Photonic Optical Sciences (IPOS), School of Physics, University of Sydney, New South Wales 2006, Australia*

**T. P. White, L. O'Faolain, T. F. Krauss**
*School of Physics and Astronomy, University of St Andrews, St Andrews, Fife, KY16 9SS, UK.*

*Corresponding author email: monat@physics.usyd.edu.au. Correspondence and requests for materials should be addressed to Christelle Monat.

**Abstract**

**Slow light has attracted significant interest recently as a potential solution for optical delay lines and time-domain optical signal processing[1,2]. Perhaps even more significant is the possibility of dramatically enhancing nonlinear optical effects[3,4] due to the spatial compression of optical energy[5,6,7]. Two-dimensional (2D) silicon photonic crystal (PhC) waveguides have proven to be a powerful platform for realizing slow light, being compatible with on-chip integration and offering wide-bandwidth and dispersion-free propagation[2]. Here, we report the slow light enhancement of a nonlinear optical process in a 2D silicon PhC waveguide. We observe visible third-harmonic generation (THG) at a wavelength of 520nm with only a few watts of peak power, and demonstrate strong THG enhancement due to the reduced group velocity of the near-infrared pump signal. This demonstrates yet another unexpected nonlinear function realized in a CMOS-compatible silicon waveguide.**

**Main text**

Although silicon has been the material of choice for the CMOS industry and more recently for integrated photonics, its optical properties – e.g light emission – still provide major challenges. In addition to an indirect band-gap and inversion symmetry, its strong absorption in the visible restricts the potential emission window to wavelengths above ~800nm. Nonlinear optical effects such as stimulated Raman scattering and THG offer new “tricks” for light emission[8], thereby extending the functionality of silicon photonics.

2D PhCs have recently attracted considerable attention by controlling the propagation of light in unprecedented ways[9,2]. In particular, they can produce “slow” light[1,2] with the ability to dramatically enhance nonlinear optical phenomena[3,4,7]. However, although nonlinear optical processes have been widely demonstrated in silicon nanowires,[10,11,8,2] corresponding demonstrations in silicon PhCs – especially with slow light – have been elusive, only having been reported in the context of the electro-optic coefficient[12].

Here, we report visible (green light) THG in slow light silicon PhC waveguides via end-fire coupling of ~ 10 W peak pump power near-infrared pulses. This power is 5 to 6 orders of magnitude lower than that of earlier THG demonstrations in bulk silicon[13,14,15,16], and arises from a combination of extreme mode confinement by the PhC waveguide, slow light enhancement, and extraction of the visible light via the PhC lattice.

The generation of third-harmonic light (electric field intensity $I_{3\omega}$, frequency $3\omega$) from a fundamental pump beam ($I_\omega$, $\omega$) propagating in a lossless homogeneous waveguide of length $L$ is given by[17]:

$$I_{3\omega} = (3\omega)^2 \cdot (\frac{2\pi}{nc})^4 \cdot I_\omega^3 \cdot L^2 \cdot (\chi^{(3)})^2 \cdot sinc^2[\frac{\Delta k(\omega)\cdot L}{2}] \cdot f(A_\omega, A_{3\omega}) \qquad (1)$$

where $\chi^{(3)}$ and $n$ are the 3rd order nonlinear susceptibility and refractive index of silicon, $\Delta k = k_{3\omega} - 3k_\omega$ is the phase mismatch between the fundamental mode and the third-harmonic wavevectors and $f(A_\omega, A_{3\omega})$ accounts for the spatial overlap between the two modes. For perfect phase matching ($\Delta k=0$) and maximum mode overlap ($f=1$), Equation (1) primarily reflects the THG cubic dependence on $I_\omega$, which arises from the basic nature of the THG process – i.e., converting three $\omega$ photons into a single $3\omega$ photon (Fig. 1a). Clearly, then, increasing $I_\omega$ within the nonlinear material is crucial to enhancing the THG efficiency. This has been achieved in the past by employing ultra-high-$Q$, small modal volume *silica* microtoroids,[18] although these tend to yield narrow bandwidth, and dispersive features. Another approach has been to exploit the high density of states at the band-edge of periodic structures in various materials and geometries such as Bragg gratings in porous silicon[19,20], 2D GaN PhCs[21] and 3D polystyrene PhCs[22]. These schemes generally involve a free-space configuration (reflection or diffraction surface probe experiments) where the lack of optical confinement limits the potential enhancement of $I_\omega$, thus requiring megawatt peak pump powers.

Combining optical confinement and dispersion engineering through the use of optimized 2D PhC waveguides[23,24,25] is highly promising because $I_\omega$ is related to the peak power ($P_\omega$) through

$$I_\omega \propto \frac{P_\omega}{A_\omega} \cdot \frac{n_g}{n} \qquad (2)$$

where $A_\omega$ and $n_g$ are the effective area and group index of the fundamental mode, repectively. Hence, by exploiting the extreme concentration of optical energy afforded by: (i) the tight confinement of light within the high index, sub-μm scale ($A_\omega$ ~ 0.4 μm$^2$) silicon PhC waveguides and; (ii) spatial pulse compression in the slow light ($v_g$=c/40) regime, we significantly reduce the peak pump power required to observe THG to 10W. In addition, the PhC structure provides a mechanism for light extraction at a wavelength that would otherwise be strongly absorbed, thereby opening the spectral emission window of silicon to the visible.

Our device consists of an 80 μm long W1 PhC waveguide in a 220nm-thick air suspended silicon slab, coupled to two tapered ridge waveguides (Fig. 1a,b). Unlike the highly dispersive slow light mode associated with the band edge of typical PhC waveguides[26,27], here the fundamental mode is engineered to display both low group velocity *and* low dispersion[24] (Fig. 2a,b). Large dispersion typically broadens and distorts short pulses, which tends to compromise the benefits of slow light for nonlinear applications. In our case, however, we focus on the spectral window (1550nm to 1559nm) where the measured group velocity of the fundamental mode[28] varies almost linearly by a factor of 4 from c/10 to c/40 (Fig. 2b), enabling us to investigate the effect of group velocity.

When launching a near-infrared 1.5ps pulse train (4MHz) into the PhC waveguide, we observe green light emitted from the surface of the chip by eye (Fig. 3a). The emission is directional, being at an angle ~ 10º from the vertical, in the backward direction, as indicated by the schematic in Fig. 1a. Imaging the emission onto a calibrated linear CCD camera with a 0.25 N.A. microscope objective reveals that it is localized above the PhC waveguide, and decays exponentially along its length (Fig. 3b). The total emitted green power (integrated spatially over the CCD image, Fig. 4) shows a cubic dependence on the coupled pump power up to ~ 65 μW and is verified to have a wavelength of 520nm ± 5nm using bandpass filters, both of which are expected for a THG process driven by a 1560nm pump. At higher pump powers, a slight saturation occurs in the fundamental power transmission (see Fig. 4) due to two-photon and subsequent free-carrier absorption. We observe a maximum THG output of ~10pW for 80μW (10W) average (peak) pump power.

In general, there are a number of effects that can contribute to a variation in the THG efficiency along the waveguide such as group velocity dispersion (GVD) and nonlinear absorption, both of which degrade the fundamental pulse intensity along the PhC waveguide. It potentially also includes phase matching between the fundamental and third-harmonic modes, although here the extremely short (~ 1μm) absorption length of the third-harmonic light in silicon dampens this effect (see Methods). In order to minimize these effects and determine the dependence of the THG efficiency solely on group velocity, we therefore restricted our measurements to a region within

5μm of the PhC waveguide entrance, which is much smaller than the dispersion length associated with the GVD, even in the "fast light" regime (see Methods).

Figure 5a,b shows that the observed THG power displays a clear enhancement for pump wavelengths near 1557nm where the group velocity is lowest. Equation (1) predicts a cubic dependence on $n_g$ of the THG power obtained at a fixed pump power. In order minimize the nonlinear loss saturation effect discussed above at all wavelengths though, we chose instead to plot on Fig. 5c,d the input power density ($P_\omega/A_\omega$) required to produce a constant (and sufficiently low) THG output power (~0.2 pW) as the wavelength (hence group index $n_g$) is varied. By plotting the power density ($P_\omega/A_\omega$) rather than power ($P_\omega$) we factor the spectral dependence of $A_\omega$ out in order to focus on the variation due solely to group index (see Methods). The results show very good agreement with a $1/n_g$ variation, as expected from Equation (2) – $P_\omega/A_\omega \propto I_\omega/n_g$ when considering a constant intensity $I_\omega$ responsible for a given THG signal. Note both the trend and the variation in enhancement is well accounted for using *only* the experimentally measured group velocity dispersion of Fig. 2b. It is clear, then, that any contribution from other effects would cause a discrepancy with experiment, even if (by coincidence) its wavelength dependence happened to be identical to that of $n_g$. Hence we believe these results conclusively demonstrate direct slow-light enhancement of this nonlinear process.

Our experiments were performed with ~10W peak pump powers, corresponding to a reduction of 5 to 6 orders of magnitude compared to previous reports[13,14,15,16] of THG in silicon. Even more significantly, this work represents a nearly 100-fold reduction in pump power relative to fully phase-matched THG in PPLN/KTP waveguides[29]. Although a comparable power density (~GW/cm$^2$) has been achieved in ultra-high Q (>10$^7$) cavities[18], the advantage of the PhC waveguide approach is that the full bandwidth of short optical pulses can be accommodated. We estimate our conversion efficiency $\eta$ to be ~$10^{-7}$ (or 5 x $10^{-10}$ for 1W of peak pump power), which represents an increase of 5 orders of magnitude over that reported in 3D polystyrene PhCs ($\eta$ ~$10^{-15}$ for 1W peak pump power as inferred from the quoted value of $\eta$ ~$10^{-5}$ at $P_{\omega}$=10MW[22]). This efficiency could be further improved, e.g. by decreasing the effective area ($\eta \propto 1/A_{eff}^{\,3}$) or the group velocity ($\eta \propto n_g^{\,3}$ ). A group velocity of c/80 can be reasonably well achieved with this PhC waveguide design[24] – this would provide an order of magnitude improvement in $\eta$. Efficiency could also be improved at high pump powers by reducing nonlinear losses (in particular due to free carriers) through techniques such as ion implantation.

Besides tight optical confinement and slow light, the 2D PhC geometry offers additional versatility to improve the third-harmonic generation and extraction efficiency. In periodic structures, the phase matching condition, $\Delta k$=0, is relaxed to $\Delta k=\pm mG$, where $mG$ can be any reciprocal lattice wave-vector, increasing the possibilities for phase matching (see Methods). Perhaps more importantly in our case, since the absorption length at $3\omega$ is extremely short (3dB/µm absorption loss at 520nm in silicon[30]), the PhC also provides a suitable platform for extracting light by coupling to surface radiating modes above the light-line. The directive nature of the emission (~$10^{o}$) as well as the absence of green emission from the access waveguides, suggests that a component of the third-harmonic Bloch mode in the PhC lies above the light line, as illustrated by the band structure in Fig. 2a. This provides a mechanism for the THG to be extracted out-of-plane. However, because the 3ω Bloch mode also contains harmonic components well confined in the PhC slab below the light line, the measured pico-watt level of green emission is expected to be significantly lower than the total THG power generated in the PhC waveguide. The conversion efficiency reported above is therefore a conservative estimate. In addition, the PhC waveguide geometry was not optimized for third-harmonic extraction in this study, so modification may well increase overall device efficiency. Finally, we note that the optimization of all of these processes can be done across a wide range of frequencies, allowing one to address the entire visible spectrum, or to extend the THG to other spectral windows.

In conclusion, we report optical third-harmonic generation of visible (green) light, enhanced by a reduction in the group velocity, or "slow light" in 2D silicon photonic crystal waveguides. We observe visible green emission for only ~10W peak pump powers due to both the tight light confinement within the PhC waveguide and the energy density enhancement provided by the slow light mode. Following recent observations of other nonlinear effects such as efficient Raman amplification and four wave mixing, the THG observed here further highlights the rich photonic functionality available with the silicon photonics platform.

**Methods**

- Device structure and fabrication

The 2D PhC structure consists of a triangular lattice of air holes with lattice constant *a*=414nm and hole radius 118nm (0.286*a*) etched into a 220nm thick silicon suspended membrane. A W1 waveguide is introduced by omitting a single row of holes along the ΓK direction to form a linear defect. The total PhC length is 80µm, and the lattice period of the first and last 10 periods is increased to 444nm parallel to the waveguide to enhance coupling to the slow light mode[31]. The dispersion of the PhC waveguide is engineered by shifting the first two rows of holes adjacent to the guide perpendicular to the direction of propagation[24]. For the waveguide used in this experiment, the first and second rows are shifted 52nm away from and 12nm toward the axis of the waveguide, respectively. Light is coupled in and out of the PhC waveguide via 2mm long ridge access waveguides whose width is tapered from 3µm to 0.7µm over 200µm close to the PhC waveguide, in order to improve coupling to the PhC. The group velocity dispersion $\beta_2$ for the engineered PhC guided mode ranges between $3 \times 10^{-21}$ to $2.5 \times 10^{-20}$ $s^2/m$ for the spectral window of interest, providing an associated dispersion length for 1.5ps pulses from 90µm to 750µm. This is longer than the entire PhC waveguide length and much longer than the small 5µm region considered in Fig. 5, and so we expect the effects of dispersion on our measuments to be negligible.

We note that this device was not optimized in terms of losses, which are dominated by coupling losses. There are several obvious routes to further improve this issue, for example through the use of inverse tapers at the end-facets. The loss of 17dB extracted from Fig. 4 is comprised of out-coupling losses (typically ~10 dB and measured to be at best of ~ 8dB), propagation loss in the ridge and nanowire segments

(~2-3dB), scattering loss at the nanowire/ PhC interface (<1 dB) and the propagation losses in the PhC waveguide in the slow light regime (2-3dB).

The device was fabricated from a SOITEC silicon-on-insulator wafer by electron-beam lithography (hybrid ZEISS GEMINI 1530/RAITH ELPHY) and reactive ion etching using a $CHF_3/SF_6$ gas mixture. The silica layer under the PhC slab was selectively under-etched using a HF solution to leave the PhC section in a suspended silicon membrane. More details of the procedure are given in Ref [32].

- Transmission experiment

The device was probed using a polarization controlled, near transform-limited, figure-of-8 fibre laser, tunable over the C-band. The pulses were $sech^2$ shaped, ~1.5ps long, with a spectral full-width-at-half maximum of ~2nm and were amplified through an Er-doped fibre amplifier. The pulses were launched into the TE-like mode of the waveguide, using lensed fibres with a 2.5µm focal length. To calculate the "coupled power" on Fig. 4 and 5 from the power launched into the input lensed fibre, we estimated an in-coupling insertion loss of 8dB. This is a typical value obtained from independent Self Phase Modulation measurements on the same waveguide. Because this coupling loss is nonetheless the lowest typically measured, our estimation of the THG efficiency represents a low, or conservative, limit of the third harmonic efficiency.

- Green light measurement

The linearised, fixed gain, CCD camera (Cohu 4910) was calibrated using a low RIN doubled Nd:YAG laser diode, with the power externally controlled by an attenuator assembly and monitored with a thermopile detector (Coherent PS10 and PowerMax meter).

- Calculations

The bandstructures in Fig. 2a were calculated with a 2D Finite Difference Time Domain (FDTD) method using effective material indices of 2.81 and 4.1 at the fundamental (~1550nm) and third-harmonic (~520nm) wavelengths respectively to account for the effects of confinement by the slab and the material dispersion of Si[30]. Calculations were performed for a lattice period of *a*= 414nm and hole radius *r*= 0.286*a*, given by the experimental parameters. The calculated dispersion curves for the fundamental mode at 1550nm are red-shifted by less than 4% relative to the experimental measurements in Fig. 2b. The bandstructure shows that several symmetric modes ($H_y$ symmetric across the waveguide, like the fundamental mode) exist at wavelengths close to 520nm that can sustain the THG emission. We believe that the third-harmonic light is most likely coupled to the refractive-like mode highlighted by the dotted red line of Fig. 2a, which has the same symmetry as, and significant overlap with, the fundamental mode at 1550nm. Observation also yields an exit angle for the third-harmonic light at ~10º from the normal which is reasonably consistent with coupling to this mode. We observe no noticeable change in exit angle with pump wavelength over the 10nm wavelength range near 1560 nm studied here, leading us to believe that there is no significant change in the third-harmonic mode over this range.

The effective mode field area ( $A_\omega$ ) of the fundamental mode was calculated using 3D Plane Wave Method (PWM) and the following equation:

$A_\omega = \frac{1}{a} * \frac{(\int_{Vol} |E|^2 dV)^2}{\int_{Vol} |E|^4 dV}$ where $E$ is the electric field amplitude of the mode and *Vol* is the volume of a unit cell of length *a* associated to the PhC waveguide. This yields an increase of $A_{\omega}$ from 0.4μm$^2$ to 0.6μm$^2$ for increasing wavelength over the range studied.

- Phase matching considerations

One might expect that, since the fundamental wavevector varies by ~10% as the wavelength is tuned over a 10nm range near 1560 nm, it may influence the wavelength variation of the THG efficiency via the phase matching term. In order to shed some light on the conclusion of our work that the observed enhancement in THG efficiency over the wavelength range studied is solely due to the group index $1/n_g$, we find it useful to compare characteristic length scales in our device. In periodic structures, the phase mismatch $\Delta k$ between the fundamental and the third harmonic modes is defined at $\pm mG$, where $mG$ can be any reciprocal lattice wave-vector. Therefore, $\Delta k < \pi/a$ (where $a$ is the PhC lattice constant) and the associated coherence (or beating) length between the two modes, $L_{coh}$, is thus always > $2a$ (~0.83μm). From the specific band structure of Fig. 2a we further expect the coherence length to be above 2μm. In silicon, since the absorption length of the third-harmonic light at 520nm is ~ 1μm < $L_{coh}$, the influence of phasematching variation on the THG efficiency in our device is expected to be negligible. Further, notwithstanding this argument, or the experimental evidence, we investigated the wavelength dependence of phasematching in our device by calculating it from the bandstructure, based on coupling to the third-harmonic mode discussed above, and assuming *no losses* at the third-harmonic wavelength, and we found that it was quite different to what was observed. Hence, for all of these reasons we believe these results conclusively demonstrate direct slow-light enhancement of this nonlinear process.

**References**


1. Krauss, T.F. Why do we need slow light? *Nature Photon.* **2**, 448-449 (2008).
2. Baba, T. Slow light in photonic crystals. *Nature Photon.* **2**, 465-473 (2008).
3. Soljacic, M. *et al*. Photonic-crystal slow-light enhancement of nonlinear phase sensitivity. *J. Opt. Soc. Am. B* **19**, 2052-2059 (2002).
4. Bhat, N. A. R. & Sipe, J. E. Optical pulse propagation in nonlinear photonic crystals. *Phys. Rev. E* **64**, 0566041-05660416 (2001).
5. Settle, M. D. *et al.* Flatband slow light in photonic crystals featuring spatial pulse compression and terahertz bandwidth. *Opt. Express* **15**, 219-226 (2007).
6. Krauss, T. F. Slow light in photonic crystal waveguides. *J. Phys. D-Applied Physics* **40**, 2666-2670 (2007).
7. McMillan, J. E. Yang, X. D. Panoiu, N. C. Osgood, R. M. & Wong, C. W. Enhanced stimulated Raman scattering in slow-light photonic crystal waveguides. *Opt. Lett.* **31**, 1235-1237 (2006).
8. Jalali, B. Teaching silicon new tricks, *Nature Photon.* **1**, 193-195 (2007).
9. Vlasov, Y. A. O'Boyle, M. Hamann, H. F. & McNab, S. J. Active control of slow light on a chip with photonic crystal waveguides. *Nature* **438**, 65-69 (2005).
10. Bogaerts, W. *et al.* Nanophotonic waveguides in silicon-on-insulator fabricated with CMOS technology. *J. Lightwave Technol*. **23**, 401-412 (2005).
11. Lin, Q. Painter, O. J. & Agrawal, G. P. Nonlinear optical phenomena in silicon waveguides: Modeling and applications. *Opt. Express* **15**, 16604-16644 (2007).
12. Jacobsen, R. S. *et al.* Strained silicon as a new electro-optic material. *Nature* **441**, 199-202 (2006).
13. Wynne, J. J. Optical third-order mixing in GaAs Ge Si and InAs. *Phys. Rev.* **178**, 1295-1303 (1969).
14. Wang, C. C. *et al.* Optical Third Harmonic Generation in Reflection from Crystalline and Amorphous Samples of Silicon. *Phys. Rev. Lett.* **57**, 1647-1650 (1986).
15. Moss, D. J. Van Driel, H. M. & Sipe, J. E. Third Harmonic Generation as a Structural Diagnosis of Ion-Implanted Amorphous and Crystalline Silicon. *Appl. Phys. Lett.* **48,** 1150-1152 (1986).
16. Moss, D. J. Van Driel, H. M. & Sipe, J. E. Dispersion in the anisotropy for optical third harmonic generation in Si and Ge. *Opt. Lett.* **14,** 57-59 (1989).
17. Boyd, R. *Nonlinear Optics*, Ch2, Academic Press (1992).
18. Carmon, T. & Vahala, K. J. Visible continuous emission from a silica microphotonic device by third-harmonic generation. *Nature Physics* **3**, 430-435 (2007).
19. Martemyanov, M. G. *et al.* Third-harmonic generation in silicon photonic crystals and microcavities. *Phy. Rev. B* **70**, 073311 (2004).
20. Dolgova, T. V. Maidykovski, A. I. Martemyanov, M. G. Fedyanin, A. A. & Aktsipetrov, O. A. Giant third-harmonic in porous silicon photonic crystals and microcavities. *JETP Lett.* **75**, 15-19 (2002).
21. Coquillat, D. *et al.* Enhanced second- and third-harmonic generation and induced photoluminescence in a two-dimensional GaN photonic crystal. *Appl. Phys. Lett.* **87**, 101106 (2005).
22. Markowicz, P.P. *et al.*, Dramatic Enhancement of Third-Harmonic Generation in Three-Dimensional Photonic Crystals. *Phys. Rev. Lett.* **92** 083903 (2004).

23. Frandsen, L. H. Lavrinenko, A. V. Fage-Pedersen, J. & Borel, P. I. Photonic crystal waveguides with semi-slow light and tailored dispersion properties. *Opt. Express* **14**, 9444-9450 (2006).
24. Li, J. White, T. P. O'Faolain, L. Gomez-Iglesias, A. & Krauss, T. F. Systematic design of flat band slow light in photonic crystal waveguides. *Opt. Express* **16**, 6227-6232 (2008).
25. Kubo, S. Mori, D. & Baba, T. Low-group-velocity and low-dispersion slow light in photonic crystal waveguides. *Opt. Lett.* **32**, 2981-2983 (2007).
26. Notomi, M. *et al.* Extremely large group-velocity dispersion of line-defect waveguides in photonic crystal slabs. *Phys. Rev. Lett.* **87**, 2539021-2539024 (2001).
27. Engelen, R. J. P. *et al.* The effect of higher-order dispersion on slow light propagation in photonic crystal waveguides. *Opt. Express* **14**, 1658-1672 (2006).
28. Gomez-Iglesias, A. O'Brien, D. O'Faolain, L. Miller, A. & Krauss, T. F. Direct measurement of the group index of photonic crystal waveguides via Fourier transform spectral interferometry. *Appl. Phys. Lett.* **90**, 261107 (2007).
29. Rusu, M. *et al.* Efficient generation of green and UV light in a single PP-KTP waveguide pumped by a compact all-fiber system. *Appl. Phys. Lett.* **88**, 121105 (2006).
30. Green, M. A. & Keevers, M. J. Optical Properties of Intrinsic Silicon at 300K. *Progress in photovoltaics research and applications* **3**, 189-192 (1995).
31. Hugonin, J. P. Lalanne, P. White, T. P. & Krauss, T. F. Coupling into slow-mode photonic crystal waveguides. *Opt. Lett.* **32**, 2638-2640 (2007).
32. O'Faolain, L. *et al.* Low-loss propagation in photonic crystal waveguides. *Electronics Lett.* **42,** 1454-1455 (2006).

**Acknowledgements**

This work was supported by the EU-FP6 Marie Curie Fellowship project "SLIPPRY", the EU-FP6 Network of Excellence "ePIXnet" and the EU-FP6 "SPLASH" project. The fabrication was carried out in the framework of the ePIXnet Nanostructuring Platform for Photonic Integration. We would also like to acknowledge the Australian Research Council (ARC) through its Federation Fellow, Centre of Excellence and Discovery Grant programs as well as the International Science Linkages program of the Australian Department of Education, Science and Technology.

**Competing financial interests**

There is no competing financial interest.

**Figure captions:**

**Figure 1 – Green light emission through third-harmonic generation in a slow light photonic crystal waveguide. a**, Schematic of slow-light enhanced third-harmonic generation. The fundamental pulse at frequency $\omega$ (energy $\hbar\omega$) is spatially compressed in the slow light photonic crystal waveguide, increasing the electric field intensity, while the third-harmonic signal, at frequency $\omega_{TH}$=3$\omega$, is extracted out-of-plane by the photonic crystal with a specific angle off the vertical direction. **b**, Scanning Electron Microscope image of the tapered ridge waveguide connected to the photonic crystal waveguide etched in a thin silicon membrane; the bar scale represents 1µm.

**Figure 2 – Photonic crystal waveguide dispersion. a**, 2D FDTD band structure calculated around 1550nm ($a/\lambda$=0.258) and 520nm ($a/\lambda$=0.77). Only symmetric modes are displayed in the upper frequency window with the dotted red line highlighting the fundamental refractive-like mode folded back into the 1st Brillouin zone ($H_y$ mode profile in the inset) that can sustain the third-harmonic. The black dashed line in the lower frequency window represents the light line while the upper frequency region lies entirely above the light line. **b**, Measured transmission and group index of the photonic crystal waveguide. The blue areas highlight the probed fundamental and third-harmonic spectral regions.

**Figure 3 – Observation of green light. a**, Visible green emission as seen by eye from the surface of the chip. **b**, Emission as captured by a 0.25NA microscope objective and imaged onto the CCD camera, with the enclosed box indicating the relative position of the PhC waveguide; the pump is injected from the left hand side. Note that the green light emission starts at the entrance of the slow PhC section (after the first 10 PhC periods stretched to enhance coupling, see Methods) and decays

exponentially along the PhC waveguide length. The bar scale on (b) corresponds to 10 μm.

**Figure 4 – Power dependence of the green light emission.** The left axis ( ● ) represents the measured visible green power as a function of the average near-infrared (IR) power coupled into the waveguide at 1556.5nm with the black solid line being a cubic fit. The error bars are derived from noise estimation on the CCD. The right axis (-×-) represents the transmitted average near-infrared power through the waveguide structure at 1556.5nm.

**Figure 5 – Slow light enhancement of green light emission. a**,**b**, Green light power as a function of coupled near-infrared peak power ($P_\omega$) for varying pump wavelengths. The constant power contour used for Fig. 5c,d appears as the dashed red line in (a). **c**,**d**, Coupled peak power density ($P_\omega/A_\omega$) of the pump needed to observe a constant third-harmonic power of 0.2pW as a function of the pump wavelength (c) and group index $n_g$ (d). The error bars are derived from noise estimation on the CCD. The solid line on (d) represents a $1/n_g$ fit expected from the $n_g$-enhancement of the optical energy density.

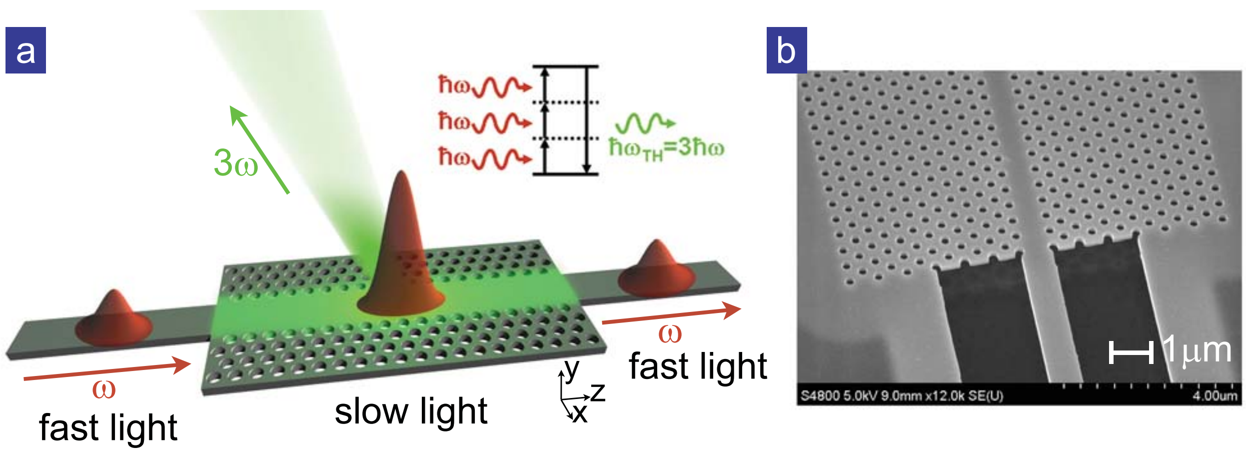
a
3ω
ħω
ħω
ħω
ħω_TH=3ħω
ω
fast light
slow light
y
z
x
ω
fast light
b
1μm
S4800 5.0kV 9.0mm x12.0k SE(U)
4.00um

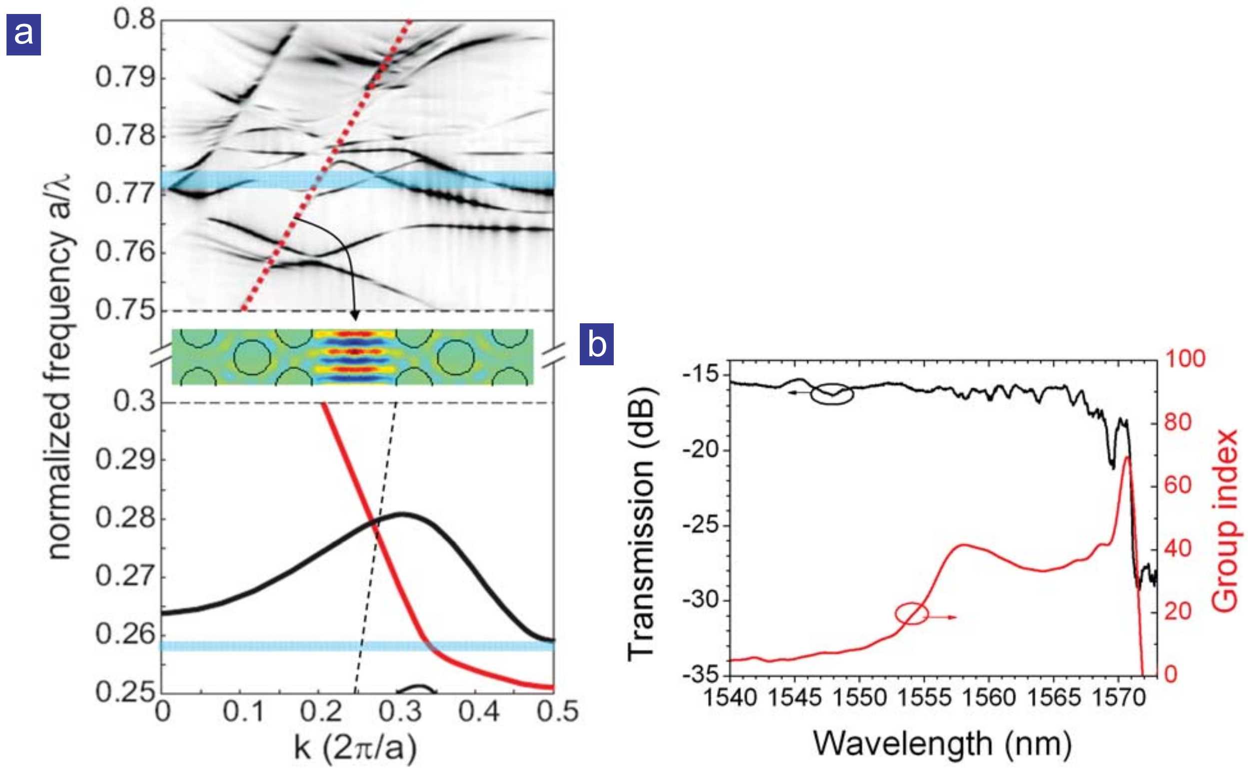
a
b
normalized frequency a/λ
0.8
0.79
0.78
0.77
0.76
0.75
0.3
0.29
0.28
0.27
0.26
0.25
0
0.1
0.2
0.3
0.4
0.5
k (2π/a)
Transmission (dB)
-15
-20
-25
-30
-35
1540
1545
1550
1555
1560
1565
1570
Wavelength (nm)
Group index
100
80
60
40
20
0

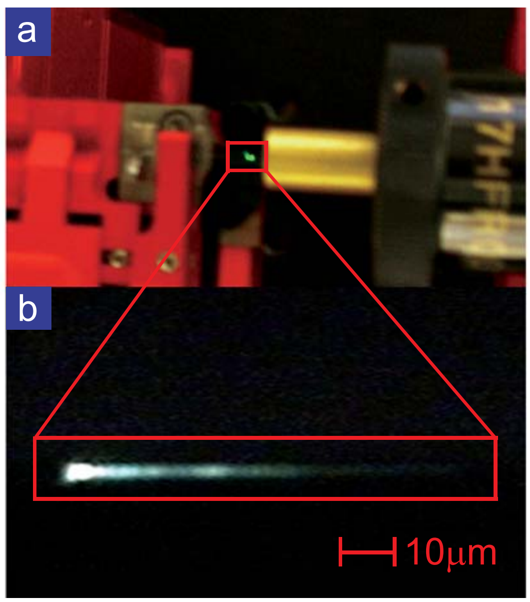
a
b
10μm

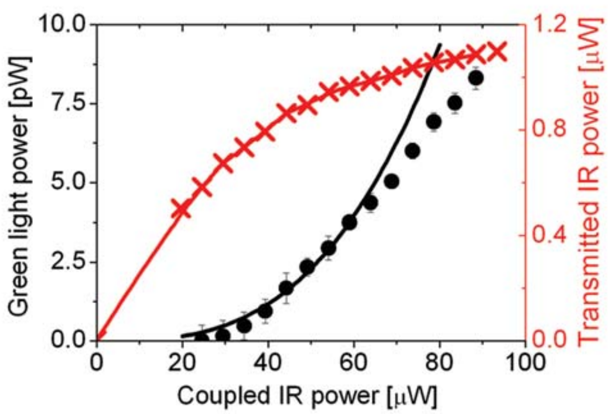

10.0
7.5
5.0
2.5
0.0
Green light power [pW]
0
20
40
60
80
100
Coupled IR power [μW]
1.2
0.8
0.4
0.0
Transmitted IR power [μW]

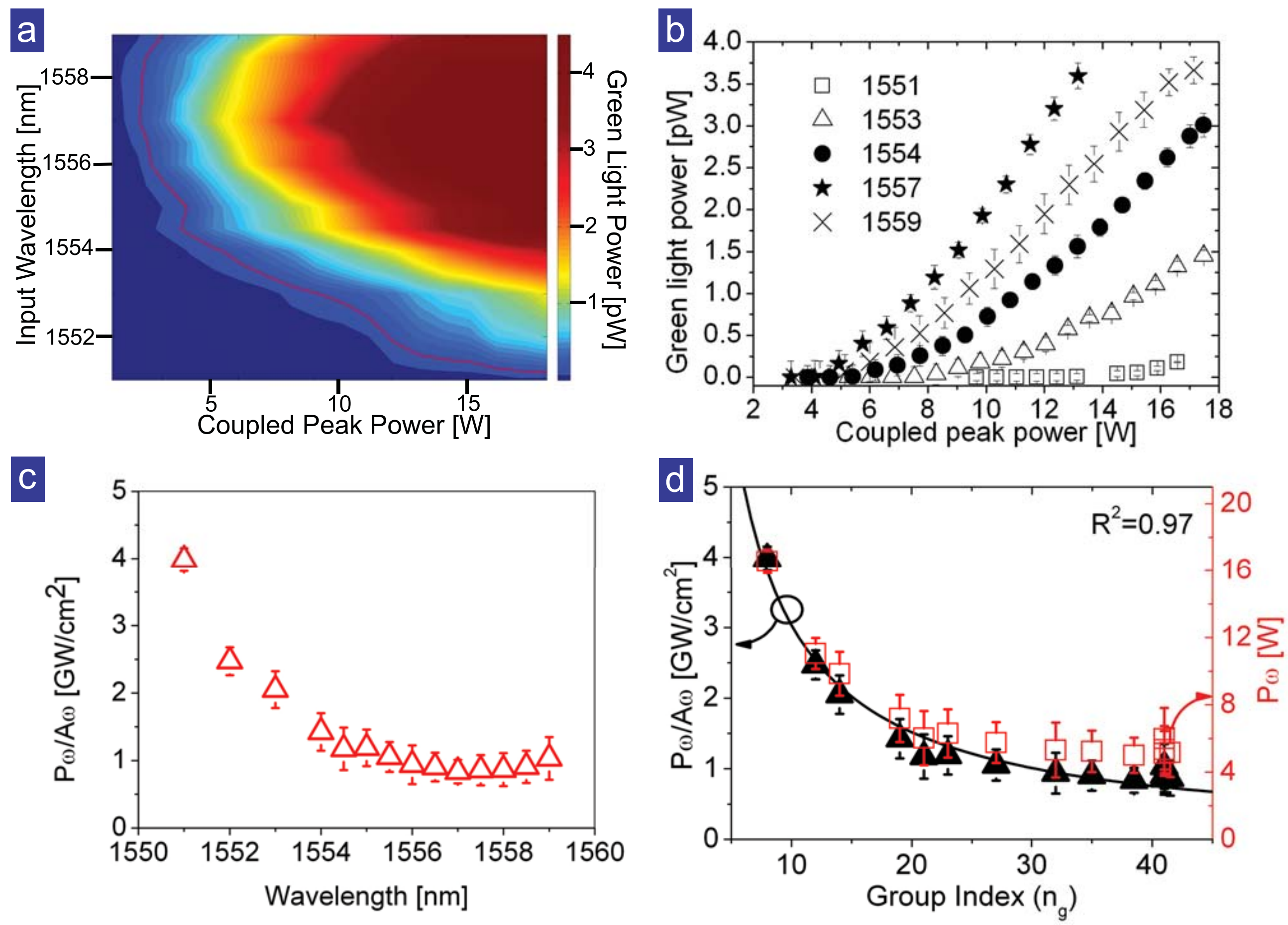
a
Input Wavelength [nm]
1558
1556
1554
1552
5
10
15
Coupled Peak Power [W]
Green Light Power [pW]
4
3
2
1
b
Green light power [pW]
4.0
3.5
3.0
2.5
2.0
1.5
1.0
0.5
0.0
1551
1553
1554
1557
1559
2
4
6
8
10
12
14
16
18
Coupled peak power [W]
c
Pω/Aω [GW/cm2]
5
4
3
2
1
0
1550
1552
1554
1556
1558
1560
Wavelength [nm]
d
Pω/Aω [GW/cm2]
R2=0.97
Pω [W]
20
16
12
8
4
0
10
20
30
40
Group Index (ng)